OPERATIONAL MODAL ANALYSIS FOR CHARACTERIZATION OF MECHANICAL AND THERMAL-HYDRAULIC FLUCTUATIONS IN SIMULATED NEUTRON NOISE

L.A Torres [(1)], V. Verma[(2)], C. Montalvo [(1)], A. Dokhane[(2)] and A. García-Berrocal[(1)]

(1) Energy and Fuels department, Universidad Politécnica de Madrid (UPM)

Ríos Rosas 21, 28003 Madrid, Spain

(2) Paul Scherrer Institut, Laboratory for Reactor Physics and Thermal-Hydraulics, CH-5232 Villigen PSI, Switzerland

ABSTRACT

In the study of the neutron noise in KWU pre-Konvoi PWRs, techniques, such as The Hilbert Huang Transform, but mainly traditional Fourier analysis is used widely to infer spectral characteristics, nevertheless these techniques exhibit important limitations in decomposing the signal so that we can distinguish the contribution of different phenomena (thermal-hydraulic and mechanical perturbations) in the same frequency range. Besides, there are difficulties to gather and present all the results in a single plot which shows the response of the core as a whole, making complex the data visualization. To overcome these limitations, an alternative methodology is researched, the so-called, Operational Modal Analysis (OMA), concretely the Frequency Domain Decomposition (FDD). This methodology is widely used in the study of the dynamic properties of systems and structures. The FDD was performed on a series of neutron noise signals from simulated scenarios based on the transient nodal code SIMULATE-3K. The simulations considered assume different sets of perturbation, from individual sources of fluctuations to combined sources. The methodology separates in the two first singular values and singular vectors the responses due to mechanical vibrations and thermal-hydraulic fluctuation in all the frequency range, in such a way that allows distinguishing different phenomena taking place at an equal frequency range as well as the increase of the response due to each phenomenon. The good performance of OMA in the present study provides promising possibilities to infer characteristics of the input excitation from the neutron noise data in PWR. Finally, the methodology shows remarkable advantages in the compilation of the results which can be utilized for monitoring purposes.

Keywords:

Operational Modal Analysis, Noise analysis, neutron noise, Simulate 3K, mechanical perturbations, thermal-hydraulic perturbations

1. INTRODUCTION

The Neutron noise is a phenomenon present in all types of nuclear reactors and it can be defined as a series of fluctuations around the mean value of a time-dependent quantity due to variations in various parameters such as coolant temperature, flow patterns, mechanical vibrations, etc, assuming the process as stationary and ergodic in time (Bermejo 2015; Runkel 1987). Therefore, neutron noise analysis can be used for diagnostic purposes as well as surveillance and monitoring in nuclear reactors (Dykin et al. 2014; Hashemian 2006; Pázsit et al. 2019).

In the first years of operation, some KWU[1] PWRs had to make automatic power reductions and install filters to mitigate neutron flux fluctuations (Runkel 1987). In the last decade, there has been a noticeable increase in neutron noise levels in certain German, Swiss, and Spanish reactors, of similar design (RSK/ESK 2013; Spanish Nuclear Safety Council 2011). This has led to a rise in the scientific interest and effort to understand its phenomenology as can be seen in different papers (Bermejo, Montalvo, and Ortego 2017; Olmo-Juan et al. 2019; Seidl et al. 2015; Tran, Pázsit, and Nylén 2015; Viebach et al. 2018, 2019).

The operational mechanisms and the internal structure of a PWR constitute a large number of possible sources of perturbations actuating at the same time. All those possible thermal-hydraulic and mechanical perturbations are under constant cross feedback, producing simultaneous changes in neutron noise and making the phenomenology a challenging matter to study (Bermejo 2015; Runkel 1987). Furthermore, in nuclear power plants, it is not possible to separate the effects of different parameters that would allow to identify the correspondence between input perturbations and the system response. These difficult particularities led to the development of simulations and methodologies to study efficiently the neutron noise (Chionis et al. 2018b, 2018a, 2020; Demazière 2011).

Here, is a highlight of recent studies focused on the influence of mechanical vibrations and thermal-hydraulic oscillations on neutron noise: (Bermejo et al. 2017; Chionis et al. 2017, 2018b, 2018a; Seidl et al. 2015; Tran et al. 2015). These studies showed that neutron noise amplitude exhibit a high dependence on the frequency domain. Flow and temperature random oscillations produce the highest response below 1 Hz and thermohydraulic fluctuations may not be the only factor with influence in the low frequency neutron noise.

In a recent contribution, simulated data was generated with SIMULATE-3K (S3K) and certain neutron spectral features were identified due to individual perturbations: mechanical vibrations, flow and temperature oscillations (Torres et al. 2019). In a recent work (Torres et al. 2020), scenarios with multiple perturbations were assumed so as to observe the effect on the neutron noise. Both studies were based on traditional Fourier analysis, which showed important limitations at inferring characteristics from the neutron noise. On one hand, it is not possible to infer which part on the neutron noise is due to which cause when there are phenomena acting in the same frequency range as it is the case of input flow and temperature perturbations simultaneously. On the other hand, the

[1] Kraftwerk Union AG with Konvoi and pre-Konvoi types

number of in-core detectors is 48, so it would be desirable for monitoring and surveillance purposes, to come up with a frequency spectrum which gathers all the information from all the detectors as a whole.

To overcome the limitations and perform better analysis, an alternative methodology was researched, the so-called, Operational Modal Analysis (OMA). This methodology is widely used in the study of the dynamic properties of systems and structures. OMA refers to modal identification methods based on response measurements only. Normally these responses of the system under study are provided by accelerometers at different locations throughout the structure (Greiner 2008; Rainieri and Fabbrocino 2015).

In real scenarios, input excitations taking place in the system are not known. Thus, in real cases, the use of OMA techniques requires a series of assumptions about the statistical character of the input excitation, e.g., white noise and gaussian distribution. (Batel and Norcross 2002; Brincker, Zhang, and Andersen 2000; Rainieri and Fabbrocino 2015). However, in simulations, all the perturbations characteristics are known a priori.

In the current study, we demonstrate the capacity and feasibility of OMA techniques to infer characteristics of the input excitation from simulated neutron noise data in a PWR by characterizing the neutron noise response. The proposed methodology was performed on a series of simulated neutron noise response measurements in the time domain. The simulated scenarios are created by different combinations of mechanical and thermal-hydraulic perturbations. Among the different OMA techniques, this work uses the Frequency Domain Decomposition (FDD), based on Singular Value Decomposition (SVD) and singular vector extraction to distinguish the different modes of vibrations.

In all the simulations, as in real plant data, a large number of signals in the time domain are recorded. Each set of signals constitute a spatial map of the response to the input perturbations. Finding suitable ways to tackle all the information is critical so that we can study the phenomenon in an efficient way. Considering these data particularities, three important advantages of the methodology can be pointed out: it provides a multi-variable and spatial analysis, allows separating the response of the system into different parts (different singular values) depending on its origin and in the same frequency region, and permits condensing a large amount of information when just a few singular values or singular vectors are plotted (Greiner 2008; Rainieri and Fabbrocino 2015). However, we also want to emphasize some particularities of the phenomenon that must be considered; we do not study vibrations as a response, but neutron noise, and we have no structural mode shapes, but singular vectors and their phase distribution.

The results obtained illustrate the effectiveness of the methodology to separate in the two first singular values the responses due to mechanical vibrations and thermal-hydraulic fluctuation in all the frequency range. Strong analogies were also identified with the traditional calculation of the coherence and phase relationships. The good performance of OMA in the present study has provided different possibilities to infer characteristics of the input excitation from the neutron noise data in PWR.

This paper is structured as follows: first, the neutron noise phenomenon and its characteristics are introduced in Section 2. Then, Section 3 explains the main limitations showed by traditional Fourier analysis and Hilbert Huang Transform. Section 4 describes

the simulations and the considered scenarios. Section 5 explains the Operational Modal Analysis and the concrete methodology utilised, i.e. Frequency Domain Decomposition, followed by presentation of the results, in Section 6. In Section 7, the results and the capabilities of the current methodology are discussed. Finally, concluding remarks are given in Section 8.

2. NEUTRON NOISE IN KWU REACTORS

The neutron flux signals recorded by neutron detectors have a constant value over time under steady-state operating conditions. Nevertheless, if the utilized measuring techniques are sensitive enough, very small fluctuations around the signal mean value can be recorded (Fry, March-Leuba, and Sweeney 1984; Hashemian 2006, 2011). These fluctuations are commonly referred as neutron noise. In a PWR core, neutron noise can be detected by a series of sensors located inside and outside the core; namely the in-core and ex-core neutron detectors. The nature of the neutron noise is stochastic, in spite of this, signal analysis techniques demonstrate that the neutron noise signals are correlated in both time and space, at a certain extent (Runkel 1987).

It is known that the small changes in the reactor neutronics are linked to the evolution of thermal-hydraulic and mechanical processes. These links and relations between the neutron noise response and the thermal-hydraulic and mechanical processes have made neutron noise a matter of study for surveillance purposes and for detecting core flow anomalies (Czibók et al. 2003; Hashemian 2006, 2011; Pázsit et al. 2019; Runkel 1987). However, the cross and simultaneous feedbacks among these three types of processes make the identification of their relationships a quite complex problem to define.

Some common spectral characteristics can be appreciated in the Konvoi and pre-Konvoi PWR neutron noise. The most remarkable characteristic is the high amplitude at very low frequencies, which contains more than 90 % of the total signal (approximately below 1 Hz). This low frequency range coincides with the frequency of maximum response due to thermal-hydraulic parameters fluctuations, the heat transfer processes, as well as the moderator temperature coefficient (MTC) feedback. Above 1 Hz, the amplitude decreases exponentially with the frequency. Then, the response is mainly affected by mechanical processes such as, the rotation of the coolant pumps and a series of vibration modes of the core Barrel (Bermejo 2015; Runkel 1987).

In multivariate analyses, an out-of-phase relationship between opposite detectors can be observed and divides the core into two halves. This feature is observable in the high frequency range. Its cause has been attributed to the vibrations of the fuel assemblies (Bermejo 2015; Dykin et al. 2013, 2014; Pázsit et al. 2019; Runkel 1987). In the case of axial phase relationship analyses, when detectors in the same string are considered, we can appreciate transport phenomena in the frequency range below 1 Hz, where thermal-hydraulic oscillations are the main contributor to the neutron noise (Bermejo 2015; Czibók et al. 2003; Runkel 1987).

In order to explain observed features, neutron noise is under research by many institutions and especially within the framework of the EU project CORTEX (Core Monitoring Techniques Experimental Validation and Demonstration). In this context, the transient

3D nodal code SIMULATE-3K (S3K) was used to perform a series of simulated scenarios that assumed only one type of perturbation in (Torres et al. 2019), and scenarios with multiple types of perturbations (Torres et al. 2020). The simulated data were analysed by means of noise analysis techniques and several spectral features were found to be similar to those of the real plant data. The main conclusions from these studies were:

- The thermal-hydraulic oscillations, on the one hand, produce the high amplitude below 1 Hz, particularly the temperature oscillations. On the other hand, they produce the linear phase difference between neutron detectors located at different axial levels, but at the same azimuthal location, due to the transport phenomenon. This linear slope depends on the ratio of amplitude between the flow and temperature fluctuations. The higher the flow perturbations, the lower the linear slope.
- When the mechanical perturbations are produced at the center of the core, it produces an out-of-phase relationship at high frequencies for detectors located at opposite sides of the direction of the vibration. This divides the reactor into two halves clearly differentiated.
- The spectral characteristics observed in the neutron noise from plant data cannot be explained by one single noise source but by a combination of all types of perturbations.

3. FOURIER ANALYSIS AND HILBERT HUANG TRANSFORM FOR PERTURBATION CHARACTERIZATION

Different types of perturbations cause different features in the neutron noise, and the effects occur in different frequency ranges. These hypotheses were the starting point to research how a decomposition methodology can help to infer characteristics from the neutron noise response. To this aim, initially, Fourier analysis and Hilbert Huang Transform were considered.

The main problem with Fourier Analysis was:

- The Fourier analysis does not allow to decompose the signal so that we can distinguish the contribution of different phenomena (thermal-hydraulic and mechanical perturbations) in the same frequency range.
- Traditional Fourier analysis does not provide efficient ways to condense the results from all detectors. We were able to calculate all the individual APSDs, but it was not possible to gather all these results in a single plot which showed the response of the core as a whole.

Hilbert Huang Transform allows to decompose signals into a series of Intrinsic Mode Functions IMF. Each IMF is centered at a certain frequency range, that is, the signal is decomposed in several spans of frequencies. Then, from the resultant IMFs, instantaneous frequency and amplitude are obtained through Hilbert transform. This is used for representing the time-frequency-amplitude spectrogram. Figure 1 shows the typical analysis with the Hilbert Huang Transform for one single signal. In the upper subfigure, the signal and the intrinsic mode functions are plotted (12 in this example). On the lower subfigure, the Hilbert spectrum constitutes the time-frequency-amplitude representation of all the intrinsic mode functions that were obtained in the decomposition.

In spite of obtaining a successful decomposition in span frequencies, this approach has some drawbacks and handicaps. The most relevant are commented as follows:

- The resultant decomposition by HHT does not provide a clear and efficient way to differentiate the scenarios or infer perturbation characteristics.
- This methodology adds a large amount of data in the decomposition, which adds more complexity to the analysis, note in Figure 1 all the data generated in the analysis of only one signal.
- The stationarity of the signals does not allow Hilbert spectrum (time-frequency-amplitude spectrograms) to contribute to the differentiation of the scenarios, or in the characterization of the perturbations. Lower Figure 1 presents the typical spectrogram obtained for all the signals in all the scenarios. The high similarity among all the spectrograms makes the differentiation of scenarios quite unfeasible through data visualization.
- The univariate approach with HHT analysis presents difficulties to analyse a spatial-multivariate scenario. It does not compile the information in an efficient way; the decomposition process adds more data without providing more information.

These handicaps and limitations motivated the research of another type of approach, based on the decomposition of the signal into different components due to the input perturbations, in this case, thermal-hydraulic and mechanical vibrations.

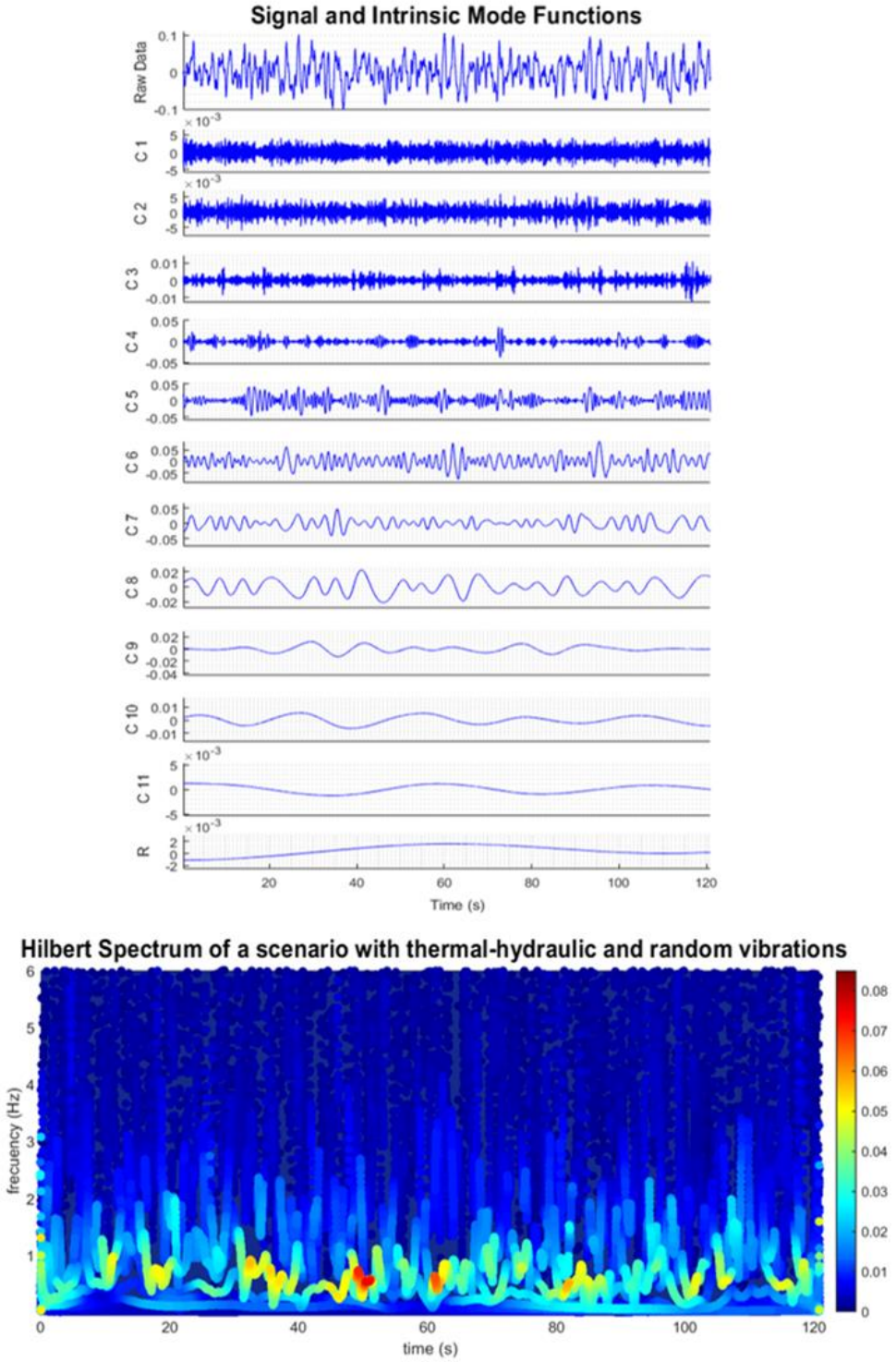

Figure 1: Typical analysis with the Hilbert Huang Transform for one single signal, in the upper side, the signals and the intrinsic mode functions (12 in this example). On the lower side, the Hilbert Huang Transform spectrum.

4. THE SIMULATIONS

This section describes the most relevant aspects of the simulations, as well as the PWR model utilised with the layout of the sensors, and finally, the scenarios considered in detail.

4.1. Simulations and sensors layout

The Paul Scherrer Institute (PSI) neutron noise methodology, including the calculation codes used for modelling and simulation of noise sources, are described here. The noise sources are based on fuel assembly vibrations, thermal-hydraulic fluctuations of inlet coolant temperature and coolant flow, and their combinations. These stochastic perturbations are modelled for a typical Westinghouse pressurized water reactor (PWR) of the OECD/NEA transient benchmark (Kozlowski and Downar 2003). It is a four-loop, 15x15 mixed core PWR comprising of 193 fuel assemblies. Radially, there are eight in-core neutron detectors, modelled at six axial levels, and four ex-core neutron detectors, modelled at two axial levels. The core layout along with the locations of in-core (O5, N12, J2, J6, G10, G14, C4, and B11) and ex-core (S1, S2, S3, and S4) azimuthal neutron detectors are shown in Figure 2. The axial levels are listed from the bottom to the top, i.e., 'Level 1' corresponds to the lowermost detector level and 'Level 6' corresponds to the uppermost detector level.

The core is modelled using the CASMO-5/SIMULATE-3 code system, and the transient calculations are performed using SIMULATE-3K (S3K). S3K is a three-dimensional transient nodal code capable of coupled neutronic and thermal-hydraulic calculations. For fuel assemblies' vibrations, the noise sources are defined in terms of assembly-wise homogenized macroscopic cross sections. As a fuel assembly oscillates in a given direction, the dynamic modification of the water-gap surrounding the fuel assemblies directly affects the time-dependent homogenized nodal two-group cross sections. The 'delta-gap model' in CASMO-5 generates perturbed two-group macroscopic cross sections corresponding to the varying water-gap. Then, the nuclear data obtained with CASMO-5 is adapted into a readable library format for the codes SIMULATE-3 and S3K for full core simulations. SIMULATE-3 performs steady-state core follow calculations and provides node-wise static fluxes and thermal-hydraulic state variables to the transient code S3K. In S3K, the 'assembly vibration model' is used to imitate simplistic lateral fuel assembly vibrations in a time-dependent manner. A detailed description of the delta-gap model and the assembly vibration model is given in a previous work (Chionis et al. 2020). In the model, all the axial nodes in the vibrating fuel assembly are displaced by the same delta-gap width. An external MATLAB script creates an include file for S3K containing time-wise delta-gap widths corresponding to the time-dependent vibration of fuel assemblies. The script allows the user to choose the vibrational characteristics of the fuel assemblies in terms of selection of vibrating fuel assemblies, their amplitude, phase and frequency of vibration. The model is able to simulate both random and sinusoidal fluctuations. Using the restart file from SIMULATE-3 calculation, S3K, performs a transient full core calculation for a certain set of operating conditions as given in the restart file to obtain three-dimensional time-dependent neutron fluxes in fast and thermal energy groups. For modelling thermal-hydraulic perturbations of inlet coolant temperature and coolant flow, S3K uses an additional module to simulate random

fluctuations in the thermal-hydraulic parameters in the four coolant loops of the reactor in a synchronous manner.

Each transient simulation with S3K is performed for a duration of 100 s at a sampling rate of 0.01 s. The output of each scenario pertaining to the noise source(s) includes responses in the form of 48 time-series signals from the in-core and 8 signals from the ex-core neutron detectors.

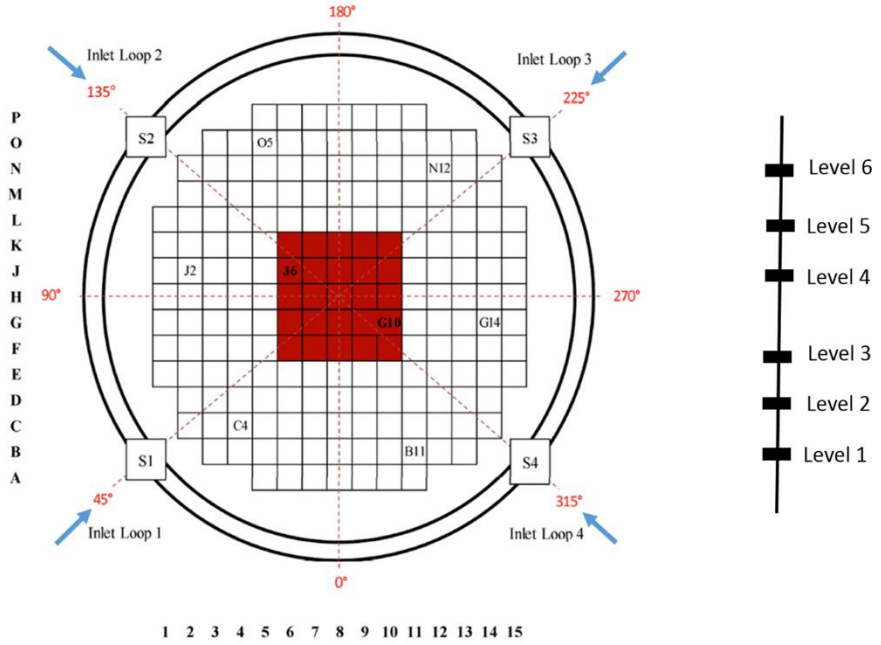

Figure 2: Radial layout of the sensor strings (i.e. O5, N12, J2, J6, G10, G14, C4, and B11), the four inlet coolant loops, and vibrating fuel elements (i.e. red boxes).

4.2. Scenarios

As mentioned, the scenarios considered are classified into three groups, basic scenarios with one type of perturbation, scenarios with multiple types of perturbations and scenarios with coloured input fuel assemblies (FA) vibrations.

4.2.1. Basic scenarios with one type of perturbation

- Temperature oscillations of ±1 °C amplitude over the mean value of 286.7 °C.
- Flow oscillations of ±1% amplitude over the nominal flow rate 100%.
- Random vibration of maximum displacement amplitude of 0.5 mm.

Thermal-hydraulic fluctuations are synchronised in the four inlet coolant loops. In the same way, all the elements of the vibrating cluster vibrate synchronously.

4.2.2. Scenarios with multiple types of perturbations

Figure 3 shows a scheme with the multiple scenarios considered and the corresponding amplitudes. These scenarios are named Scenarios M1 to M5.

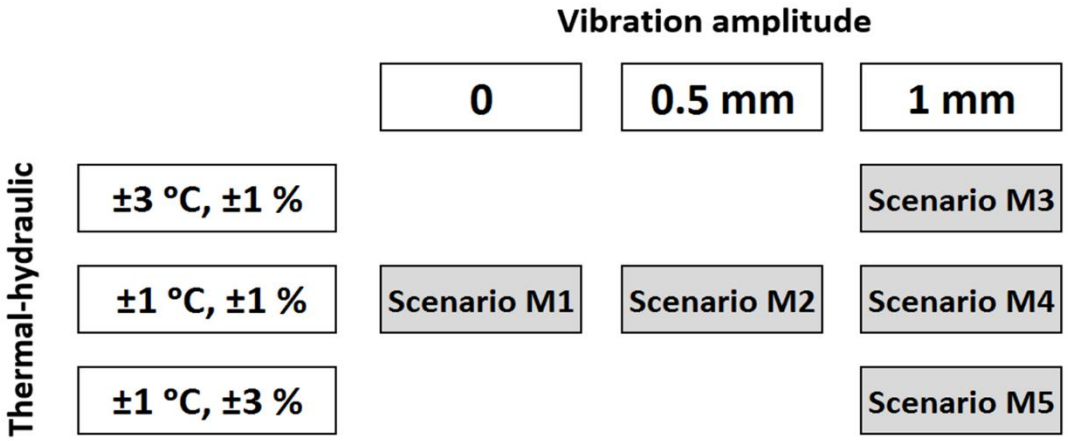

Figure 3: Scenarios with multiple perturbations. The first column indicates the thermal-hydraulic fluctuations amplitude and the first row indicates the amplitude of the vibrations assumed.

4.2.1. Scenarios with coloured input FA vibrations

Two type of scenarios are considered in this type; individual 1.5 Hz FA vibrations and 1.5 Hz FA vibrations combined with flow and temperature perturbations.

5. OPERATIONAL MODAL ANALYSIS: FREQUENCY DOMAIN DECOMPOSITION (FDD)

Operational Modal Analysis (OMA) is widely used in the study of the dynamic properties of systems and structures. It is referred to modal identification methods based on response measurements only. The present publication focuses on the use of Frequency Domain Decomposition (FDD). This method was originally applied to Frequency Response Functions (FRFs) to point out its ability to detect multiple roots and, therefore, the possibility to count the number of dominant modes at a certain frequency (Batel and Norcross 2002; Brincker et al. 2000; Greiner 2008; Rainieri and Fabbrocino 2015).

This approach is based on the fact that modes can be estimated from the spectral densities. This nonparametric technique estimates modal parameters directly from signal processing calculations. The FDD technique estimates the modes using a Singular Value Decomposition (SVD) of each of the spectral density matrices. This decomposition corresponds to a Single Degree of Freedom (SDOF) identification of the system for each singular value. In general terms, the basis of modal analysis from an experimental point of view is the denominated system equation. Denoted in time domain:

$$y(t) = g(t) * x(t) \qquad (1)$$

It connects the excitation input $x(t)$ to the measured system response $y(t)$ via the Impulse Response Function (IRF) $g(t)$ of the system using convolution:

$$[g * x](t) = \int_{-\infty}^{\infty} g(\tau)x(t-\tau)d\tau \tag{2}$$

t is the time variable integrated from $-\infty$ to $+\infty$. Convolution can be interpreted as the amount of overlap two functions have as they are shifted over each other. In the case of multi-dimensional inputs and outputs, *g(t)* is a matrix of IRFs.

Some assumptions about the input are needed. If the input is white noise, the equations are simplified, but this is rarely the case since the excitation often has a spectral distribution of its own. Additionally, noise and eventual spurious harmonics due to rotating equipment are observed in the detectors signals. Thus, in the general case, the system under study or structure is assumed to be excited by unknown forces that are the output of the so-called excitation system loaded by white noise. Under this assumption, the measured response can be interpreted as the output of the combined system, made by the excitation system and the structure under test in series, to a stationary, zero mean, Gaussian white noise (Rainieri and Fabbrocino 2015, Chapter 4).

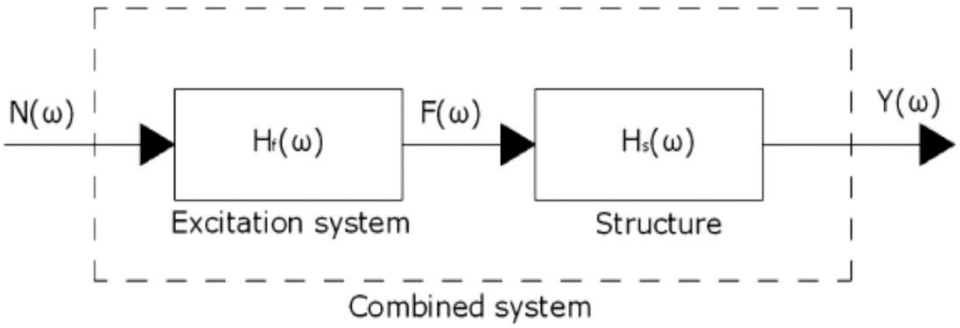

Figure 4: Combined system to explain assumptions of the input forces in OMA technique. Taken from (Rainieri and Fabbrocino 2015, Chapter 4).

By Fourier transform, equation (1) becomes in frequency domain:

$$Y(j\omega) = H(j\omega)X(j\omega) \tag{3}$$

Where *H(jω)* contains the set of Frequency Response Functions (FRFs) of the system. When both input *X(jω)* and output *Y(jω)* are known, the FRFs can directly be calculated and used for model extraction. Since *X(jω)* is not known in OMA, further mathematics and assumptions are needed.

Analogously, equation (1) can be expressed in terms of power spectral densities:

$$G_{yy}(j\omega) = |H(j\omega)|^2 G_{xx}(j\omega) \tag{4}$$

Where G_{yy} and G_{xx} are the power spectral density (PSD) of the output and input respectively. PSD is defined as the Fourier transform of the auto correlation signal. The Integral of the PSD over a certain frequency range denotes the energy contained in the signal at that frequency range.

When the PSD is calculated in a single signal, it is denominated auto power spectral density (APSD), but in the case of considering two different signals, we call it cross power spectral density (CPSD).

The PSD matrix of inputs G_{xx} is unknown in OMA and G_{yy} is the PSD matrix of measured response channels. The dimension of G_{yy} is *nxn*, being *n* the number of the measurement channels considered.

The PSD matrix G_{yy} is arranged as follows:

$$G_{yy}(j\omega)_i = \begin{bmatrix} APSD_{11} & CPSD_{12} & \cdots & CPSD_{1n} \\ CPSD_{21} & APSD_{22} & \cdots & CPSD_{2n} \\ \vdots & \vdots & \ddots & \vdots \\ CPSD_{n1} & CPSD_{n2} & \cdots & APSD_{nn} \end{bmatrix}_i \tag{5}$$

Using (3) and (4), it can then be shown that $H(j\omega)$ relates the Power Spectral Density (PSD) matrices of input and output signals as follows:

$$\left[G_{yy}(j\omega)\right] = \left[H^*(j\omega)\right]\left[G_{xx}(j\omega)\right]\left[H^T(j\omega)\right] \tag{6}$$

In the case of stationary and white noise input, G_{xx} is constant, we call it C hereafter. Only by assuming that the input is effectively represented by a constant value, we obtain relevant results. It is therefore important to realize how this input assumption will be crucial to the technique.

The FRF can be expressed in partial fraction as:

$$\left|H(j\omega)\right| = \sum_{k=1}^{n} \frac{[R_k]}{j\omega - \lambda_k} + \frac{[R_k]^*}{j\omega - \lambda_k^*} \tag{7}$$

with

$$\lambda_k = -\sigma_k + j\omega_{dk} \tag{8}$$

being *n* the total number of modes, ω_k being the pole of the k_{th} mode, σ_k the modal damping and ω_{dk} the damped natural frequency of the k^{th} mode. $[R_k]$ is called the residue

matrix consisting of mode shape vector ϕ_k and modal participation vector γ_k. All those parameters are specified for the k^{th} mode.

$$[R_k] = \phi_k \gamma_k^T \tag{9}$$

The transfer function matrix *[H]* is symmetric and an element $H_{pq}(j\omega)$ of this matrix is then written in terms of the component $r_k(p,q)$ of the residue matrix as follows:

$$\left|H_{pq}(j\omega)\right| = \sum_{k=1}^{n} \frac{r_k(p,q)}{j\omega - \lambda_k} + \frac{r_k(p,q)^*}{j\omega - \lambda_k^*} \tag{10}$$

Using expression (6) for the matrix G_{yy} and the Heaviside partial fraction theorem for polynomial expansions, we obtain the following expression for the output PSD matrix:

$$[G_{yy}(j\omega)] = \sum_{k=1}^{n} \frac{[A_k]}{j\omega - \lambda_k} + \frac{[A_k]^*}{j\omega - \lambda_k^*} + \frac{[B_k]}{-j\omega - \lambda_k} + \frac{[B_k]^*}{-j\omega - \lambda_k^*} \tag{11}$$

where $[A_k]$ is the kth residue matrix of the matrix G_{yy}. The matrix G_{xx} is assumed to be a constant value C, since the excitation signals are assumed to be uncorrelated zero mean white noise in all the measured DOFs. This matrix is Hermitian and is described in the form:

$$[A_k] = [R_k] C \sum_{s=1}^{n} \frac{[R_s]^H}{-\lambda_k - \lambda_s^*} + \frac{[R_s]^T}{-\lambda_k - \lambda_s} \tag{12}$$

The contribution of the residue has the following expression:

$$[A_k] = \frac{[R_s] C [R_s]^H}{2\sigma_k} \tag{13}$$

Considering a lightly damped model, we have the following relationship:

$$\lim_{damping \to light} [A_k] = [R_k] C [R_k]^T = \phi_k \gamma_k^T C \gamma_k \phi_k^T = d_k \phi_k \phi_k^T \tag{14}$$

where d_k is a scalar constant.

The contribution of the modes at a particular frequency is limited to a finite number (usually 1 or 2). The response spectral density matrix can then be written as the following final form:

$$G_{yy}(j\omega) = \sum_{k=1}^{n} \frac{d_k \phi_k \phi_k^T}{j\omega - \lambda_k} + \frac{d_k^* \phi_k^* \phi_k^{*T}}{j\omega - \lambda_k^*} \tag{15}$$

where n denotes that only dominant modes at a certain frequency ω are relevant. d_k is a scalar constant depending on the modal participation factor and the unknown volume of the input noise. Since mode shapes in a modal model are generally unscaled, d_k is not of further interest in pure OMA. A direct link between the measurement data G_{yy} and the modal parameters ϕ_k and λ_k is established. ϕ_k is the mode shape vector and λ_k is a complex value, which contains the natural frequency and the damping ratio.

This final form of the matrix is then decomposed into a set of singular values and singular vectors using the Singular Value Decomposition technique (SVD). This decomposition is performed to identify single degree of freedom models of the problem.

The singular value decomposition of an mxn complex matrix A is the following factorization:

$$A = U \Sigma V^H \tag{16}$$

where U and V are unitary and Σ is a diagonal matrix that contains the real singular values in descending order. For a Hermitian and positive definite matrix, such as the PSD matrix G_{yy}, it follows that U and V are identical and the decomposition can be rewritten as:

$$G_{yy} = U \Sigma U^H \tag{17}$$

The singular value decomposition is performed for each of the matrices at each frequency.

The number of nonzero elements in the diagonal of the singular matrix corresponds to the rank of each spectral density matrix. The singular vectors correspond to an estimation of the mode shapes and the corresponding singular values are the spectral densities of the SDOF system expressed in Equation (17).

If only one mode is dominating at a particular frequency, then only one singular value will be dominating at this frequency. In the case of close or repeated modes, there will be as many dominating singular values as there are close or repeated modes.

In case of resonance, only one or a few close modes contribute to the motion. Thus, there is only one term in eq. (17), which means that there is only one singular value dominating in the SVD and the corresponding singular vector is an estimate of the mode shape for that resonance frequency. Therefore, the first singular vector is a good approximation of the mode shape vector for that frequency.

Therefore, the decomposition in singular values is able to differentiate into dominant and non-dominant vibrational modes. Since the input perturbations are known, links between singular values and perturbations amplitude can be made. Besides, singular vectors contain spatial information of the contribution of each vibrational mode in each detector. It is important to mention that the different components of the singular vectors are complex numbers, therefore they have modulus and phase. The phase observed in each component gives information on the mode shape at that particular detector. So, depending on the characteristics of the singular vectors, conclusions can be drawn from the type of phenomena causing that mode of vibration.

6. RESULTS

It is important to mention some considerations regarding the detectors selected for the present results section:

- All the simulated sensors have equal characteristics, but they do not sense the perturbations equally due to their location in the core and the different distances from the sources of perturbations. In Figure 2, we can observe the different radial positions of the strings with respect to the sources of perturbations.
- The strings (J06 and G10) are located inside the vibrating cluster and exposed to the inlet coolant flow, so they are an interesting and representative location to assess the response.
- For the application of the methodology, the detectors selected can be located at the same axial level and different radial positions or different axial levels and the same radial position. The former will be referred as radial analysis and the latter as axial analysis.
- In the case of the axial analyses, Level 2 exhibits the highest response amplitude (APSD) in most cases. This can be explained by the contribution of cross flows from the downcomer. The cross flow effect is particularly important in the lower part of the core and that could explain the high values found in real data. Nevertheless, to study in detail the changes throughout the reactor, the analyses were performed in all the possible axial and radial locations.
- The methodology can extract as many singular values as the number of detectors are considered in the analysis. Nevertheless, those singular values which are very low are not plotted in the figures since they correspond to non-dominant or negligible vibrational modes. Due to this, only the first three singular values are plotted in this section.

The following results are a summary that shows and illustrates the main characteristics found. It also demonstrates the potential and feasibility of the methodology for characterizing and locating in-core perturbations using neutron noise signals. The section is organised in three subsections according to the complexity of the simulated perturbations. The first subsection presents the features that correspond to each type of

perturbation separately. The second illustrates and describes the resulted response when multiple perturbations are assumed in the scenarios. The third subsection shows the effect on the response when the amplitude of the perturbation is varied. Finally, there is a last subsection about the scenarios with FA coloured input vibrations. Each subsection presents the results which are based on the singular values and the singular vectors. The axial analysis considers the six detectors of the string J06, the radial analysis the eight detectors at level 2.

In order to understand the figures shown in this section, some indications need to be given on the two types of the presented plots. On one hand, singular value plots give information on the predominant vibration causing in the neutron noise response. The higher the difference between singular value 1 and the rest, the most predominant that mode of vibration is.

On the other hand, there are singular vector phase plots. This type of plot is similar to a phase CPSD plot but it is not the same and it requires some explanation. Each singular value has an associated singular vector. Singular value represents the amplitude of a certain vibration and the singular vector represents how this vibration manifests itself in each detector. So, in this sense, what it matters, it is the phase in the singular vector. For instance, if the singular vector at a particular frequency has 6 components, each of them represent a detector. If the first component has zero phase and the sixth component has 180 degrees phase, this means that both detectors are registering the same vibration, since both phases correspond to the first singular vector at that frequency but each one "see" the vibration at a different phase, in this case there is a phase difference of 180 degrees.

6.1. Scenarios with only one type of perturbation

Following the structure mentioned above, this subsection presents the scenarios with only one single type of perturbation at a time.

6.1.1. Thermal-hydraulic fluctuations

Only one type of perturbation is assumed, the amplitudes of temperature and flow fluctuations are ±1 ^{o}C, ±1 %, respectively.

Figure 5 shows the first three singular values for both scenarios, with temperature and flow fluctuations. To illustrate the most relevant observations, we illustrate the case of axial analysis in both cases. We can appreciate common characteristics:

- The first singular value is clearly larger than the others below 1 Hz.
- Above 3.5 Hz the difference between the singular values is constant and the decrease of all the singular values is exponential.

We can notice some differences between both scenarios:

- In the temperature scenario, the three singular values are closer to each other in all the frequency range than in the flow scenario.
- In the flow scenario, the first singular value is considerably separated from the singular values 2 and 3.

- Below 1 Hz, singular value 1 is more protruded in the temperature scenario than the flow scenario.
- The singular value 1 in temperature scenario shows a sharper decrease in amplitude around 1 Hz compared to that of flow scenario.

The difference between the first and second singular values in the frequency range in both cases demonstrates that, depending on the type of the perturbation, there is a predominant response in different frequency ranges. In the case of the temperature fluctuations, the difference between the first and the other singular values is large only below 1 Hz, while in the case of flow fluctuations, the first singular value is clearly predominant in all the frequency range. By using only traditional Fourier based methods, it is not possible to distinguish these two cases.

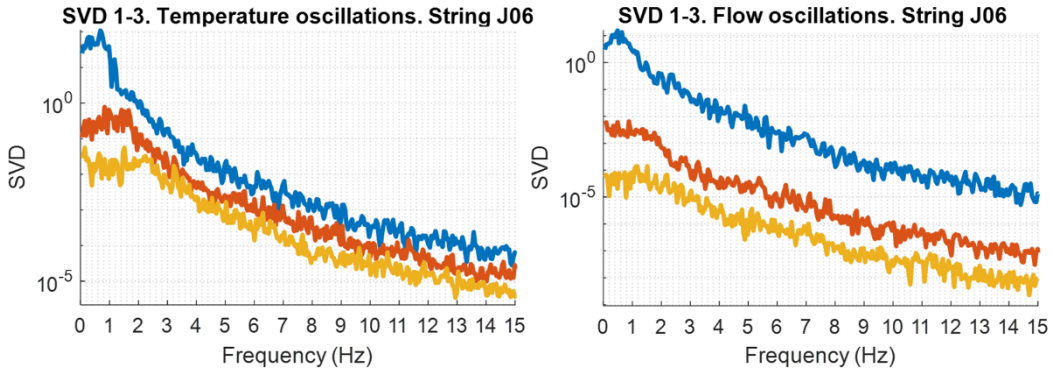

Figure 5: Singular values 1 to 3 in scenarios with only one type of perturbation, Temperature fluctuations in the left-hand side and flow fluctuations in the right-hand side (string J06).

Figure 6 presents the axial and radial singular vector analyses. Temperature fluctuations in the left-hand side and flow fluctuations in the right-hand side. Axial analyses in the first two rows, radial analyses in the third and fourth rows

In the axial analyses, upper side Figure 6, we can mention:

- A common characteristic in both cases is the presence of a linear slope in the low-frequency range (below 1 Hz approximately) for all the phases in the singular vector 1.
- In the case of the temperature fluctuation scenario, the phases exhibit a higher slope.
- The phases in the second singular vector do not exhibit patterns that add recognisable information.

In the radial analyses, lower side Figure 6, we can remark the following features:

- In both cases, the phase is the same in the first singular vector for all the frequency range. There is no transport phenomenon in the radial direction.
- Again, the second singular vector do not exhibit patterns that add recognisable information.

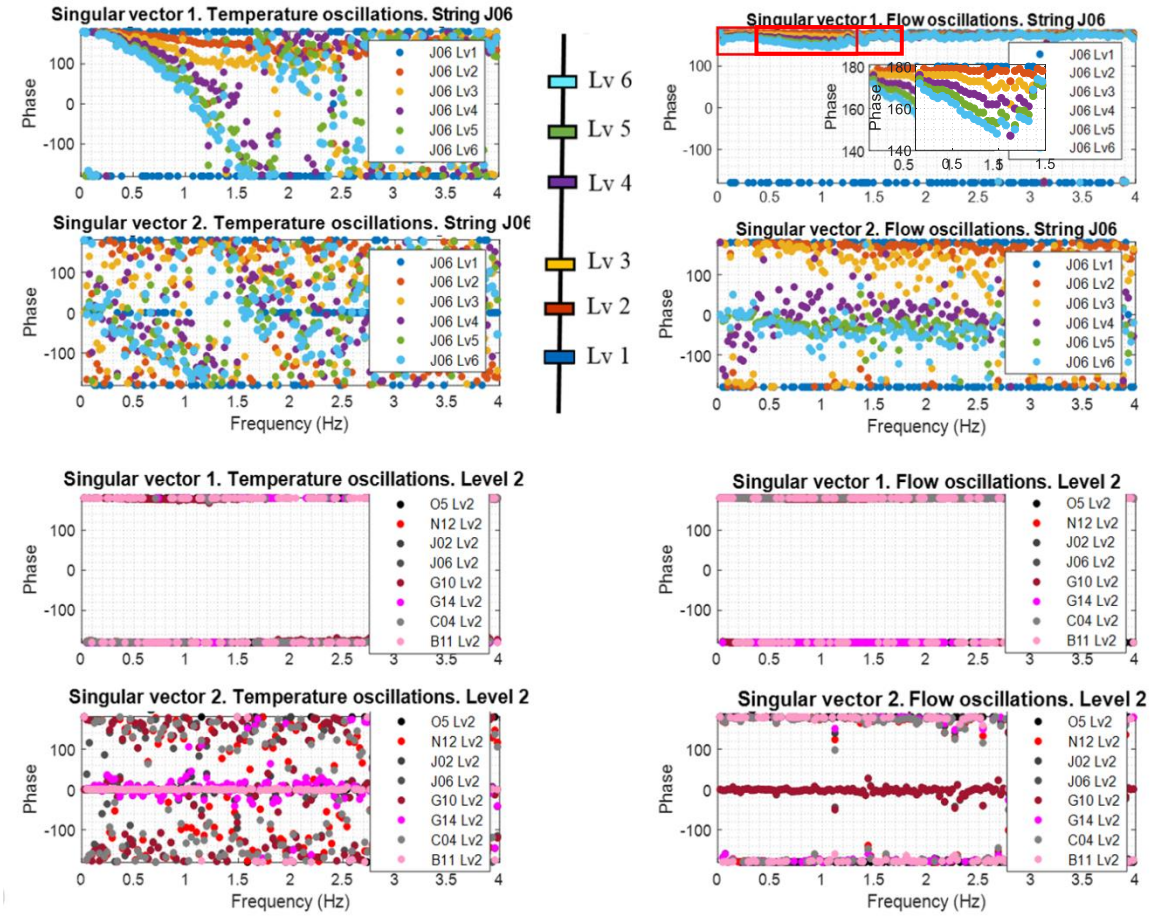

Figure 6: Singular vectors 1 and 2 in scenarios with only one type of perturbation, temperature fluctuations in the left-hand side and flow fluctuations in the right-hand side. Axial analyses in the first row and radial analyses in the second row.

6.1.2. Fuel Assembly Random vibrations

In this subsection, random vibrations of the central cluster (5x5 fuel elements) are assumed as the only type of perturbation in the core. The amplitude of vibrations is 0.5 mm.

The singular values present a very similar behaviour in axial and radial analysis. Figure 7 presents the first three singular values in the axial analysis. We can remark the following observations:

- The singular values are almost constant in all the frequency range.
- The first singular value is the most important by far. This indicates that the Fuel mechanical vibrations of the fuel assemblies are dominant in all the frequency range.

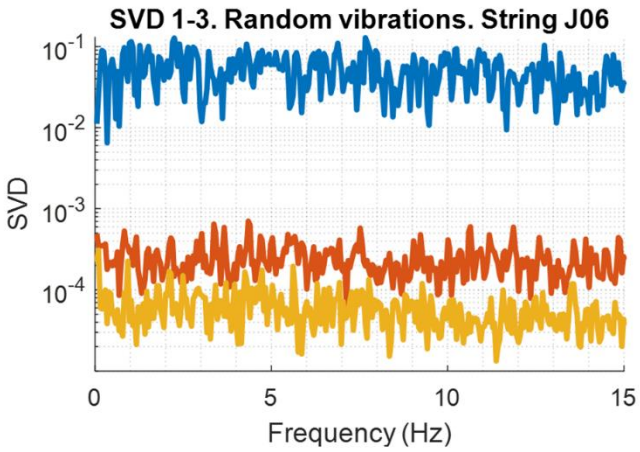

Figure 7: Singular values 1 to 3 in scenario with random vibration (radial analysis with level 2 detector)

Figure 8 shows the phase of the singular vectors 1 and 2, with axial analysis in the upper side and radial analysis in the bottom side. The following are the main differences between these two analyses:

- In the axial analyses, i.e. Figure 8 upper side, all the elements in singular vectors 1 have the same phase in all the frequency range. There is no transport phenomenon in these scenarios. The reactor is in phase in the longitudinal direction.
- In radial analysis, Figure 8 lower side shows that the reactor is divided in two zones behaving in an out-of-phase manner.
- The second singular vector does not show patterns that add recognisable information.

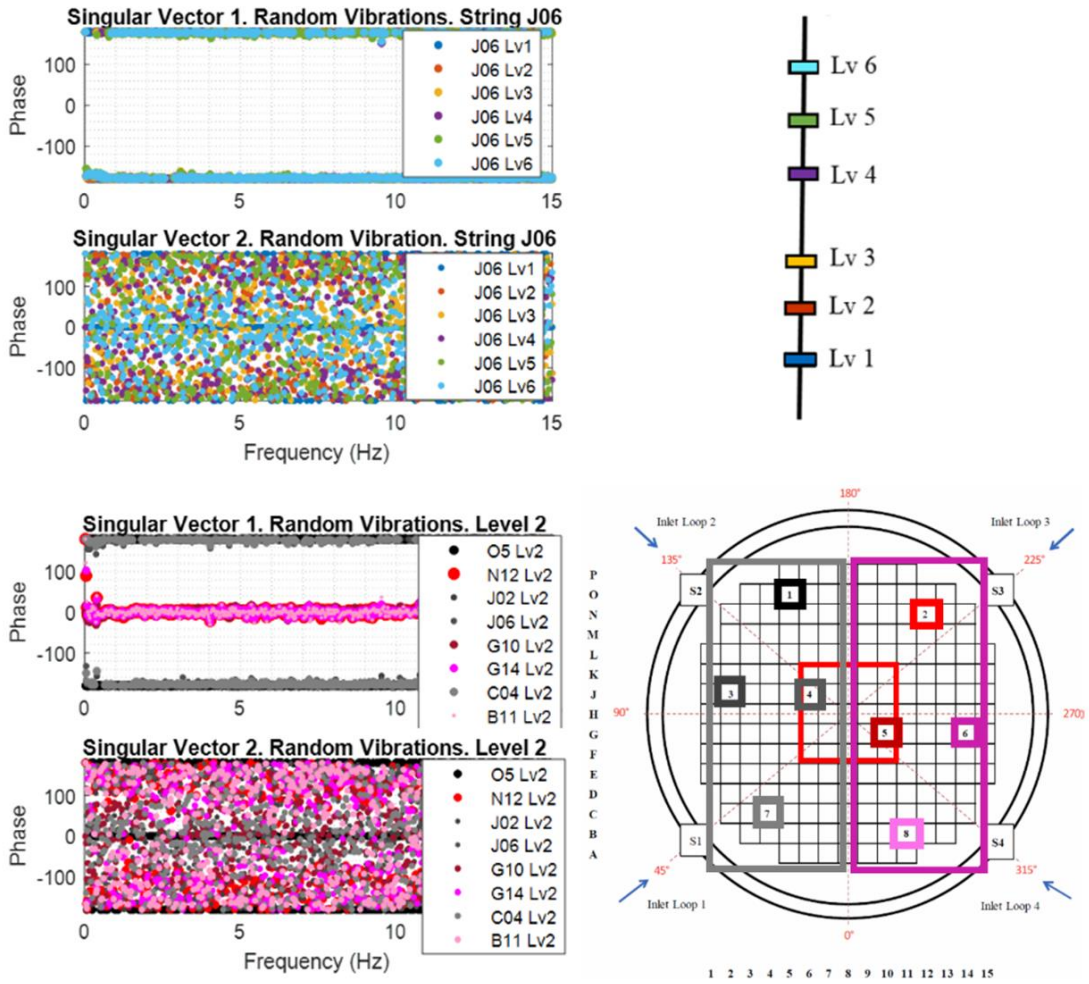

Figure 8: singular vectors 1 and 2 in scenarios with random vibrations. Radial analysis upper side and axial analysis in the lower side.

6.2. Scenarios with multiple perturbations

This subsection illustrates the resultant neutron noise response when we have multiple perturbations. In subsection 6.1 we have seen that the response due to thermal-hydraulic oscillations has a similar pattern, clearly differentiated from the scenario with random vibrations of fuel assemblies.

To illustrate the interaction among the different perturbations, in the first place, we focus on the scenario that combines temperature and flow fluctuations at a time. Then, we present the scenario that combines the two thermal-hydraulic perturbations with the FA random vibrations.

6.2.1. Temperature and flow fluctuation

Temperature and flow fluctuations are assumed to be ±1 ºC and ±1 %, respectively. Figure 9 shows the three first singular values in the axial analysis in the left-hand side, and radial analysis in the right-hand side. The characteristics of this scenario resemble those of the scenario with temperature fluctuations. We can highlight the following characteristics:

- The ratio amplitude between singular value 1 and 2 is more similar to the one in the temperature scenario than to the flow scenario
- The order of magnitude of the first singular value below 1Hz is similar to the first singular value in the scenario with only temperature fluctuation.

To understand these observations, it is important to mention that the response amplitude due to ±1 ºC fluctuations is much larger than in the case of ±1 % flow fluctuations.

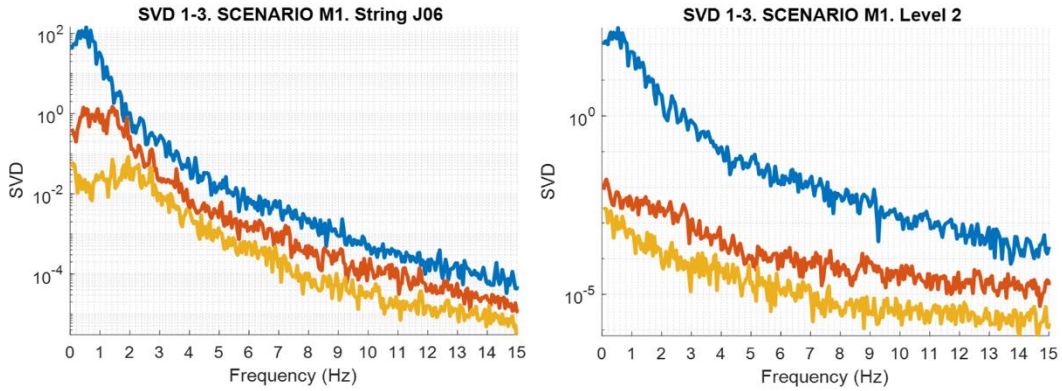

Figure 9: Singular values 1 to 3 of the scenario with temperature fluctuations and flow fluctuations. Axial analysis in the left-hand side. radial analyses in the right-hand side.

Figure 10 shows the singular vectors 1 and 2 for the scenario with the combination of temperature and flow fluctuations, with axial analysis in the left-hand side and radial analysis in the right-hand side. The most relevant characteristics are the following:

- All the first singular vector phases present a clearly linear slope in the low-frequency range in the axial analysis, Figure 10 left-hand side.
- Note that the resultant slope resembles to that of the temperature fluctuation scenario.
- The phases of the second singular vector exhibit a linear behaviour below about 1 Hz, but dispersed. However, these patterns did not add recognisable information.
- In the radial analyses, i.e. Figure 10 right-hand side, all the phases in the first singular vector are the same for all the frequency range. There is no transport phenomenon in the radial direction. The phases in the second singular vector exhibit a diffuse trend.

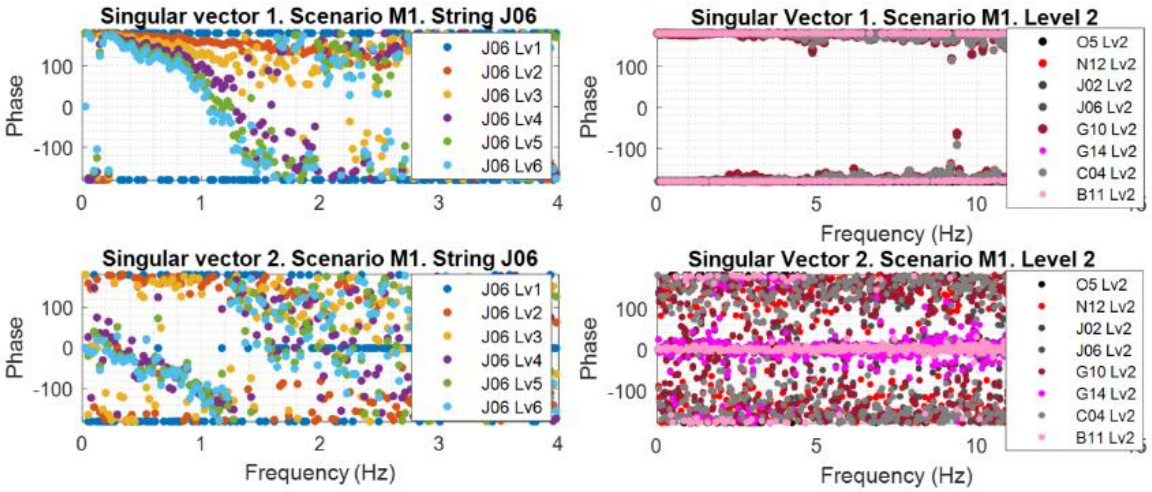

Figure 10: Singular vectors 1 and 2 of the scenario with only temperature fluctuations and flow fluctuations. Axial analysis in the left-hand side. radial analyses in the right-hand side.

6.2.2. Temperature and flow fluctuation with random vibrations

The current scenario combines temperature and flow fluctuations with random vibrations of fuel assemblies with corresponding amplitudes of ±1 ºC, ±1%, and 1 mm, respectively. In Figure 11, it can be seen the singular values 1 to 3 for the axial analysis in the left-hand side, and radial analysis in the right-hand side.

The following observations can be highlighted for the axial analysis, i.e. from Figure 11 right-hand side:

- Up to approximately 3 Hz the first singular values are very similar to those in scenario with thermal-hydraulic fluctuations.
- Above 3 Hz the first singular value exhibits a horizontal section. This happens when the response of the amplitude of mechanical vibrations of fuel assemblies exceeds that of the thermal-hydraulic one, this is discussed in Section 6.4.
- The singular value 2 behaves in the opposite way, that is, the horizontal section is below 3 Hz, while above 3 Hz the behavior resembles the case with thermal-hydraulic fluctuations, we can appreciate the characteristic exponential decrease.
- The singular value 2 and 3 do not show appreciable changes compared to the scenarios with only thermal-hydraulic fluctuations.

As seen in Figure 11, singular values 1 and 2 are divided into two sections separated by a transition zone around 3 Hz. This transition zone separates the response due to thermal-hydraulic and mechanical perturbations in both singular values.

In the case of the axial analysis, Figure 11 left-hand side, presents a very similar behaviour to the radial one, but the transition zone is approximately located around 2 Hz.

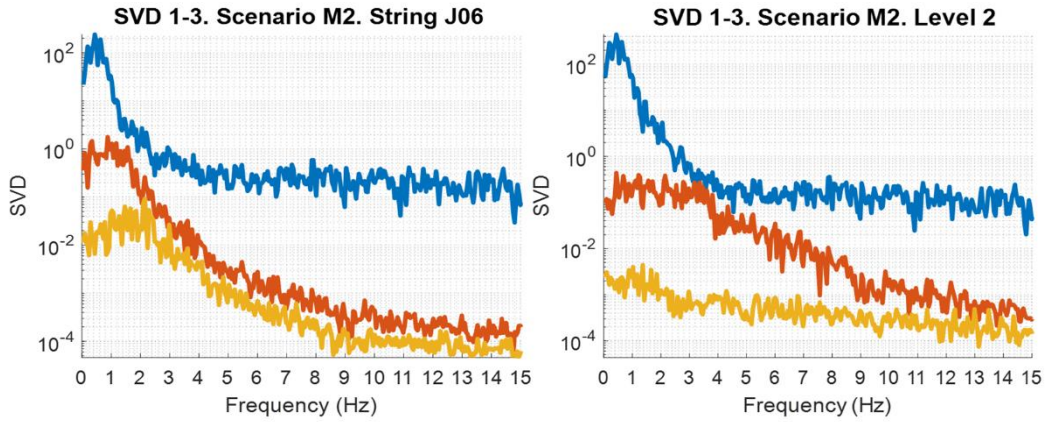

Figure 11: Singular values 1 to 3 of the scenario with temperature and flow fluctuation with random vibrations. Axial analysis in the left-hand side and radial analysis in the right-hand side.

Figure 12 shows the singular vectors 1 and 2 for the scenario that assumes temperature and flow fluctuations with FA random vibrations, axial analysis in the upper side, radial analysis in the lower side.

In the case of the axial analysis, Figure 12 upper side, we can appreciate very similar characteristics to the scenarios with temperature fluctuations, that is:

- The high slope in the low frequency range resembles that of the scenarios with temperature fluctuations.
- The phases in the singular vector 2 exhibit linear behaviour, they are dispersed and these patterns do not add recognisable information.

In the radial analysis, Figure 12 lower side, we can remark:

- The existence of two clear zones, the first zone up to approximately 4 Hz, and the second one starts from 6 Hz and onwards. In between, there is a transition zone.
- In the first zone of the singular vector 1, all the sensors have the same phase, in the second zone, the phases are separated into two groups that divide the reactor into two halves in out-of-phase.
- This separation also occurs with singular vector 2, but in an opposite way giving us a hint about the partial separation of the response due to vibrations and thermal-hydraulic fluctuations.
- It seems that the effect FA vibrations are dominant for singular vector 2 at lower frequencies below 4 Hz.

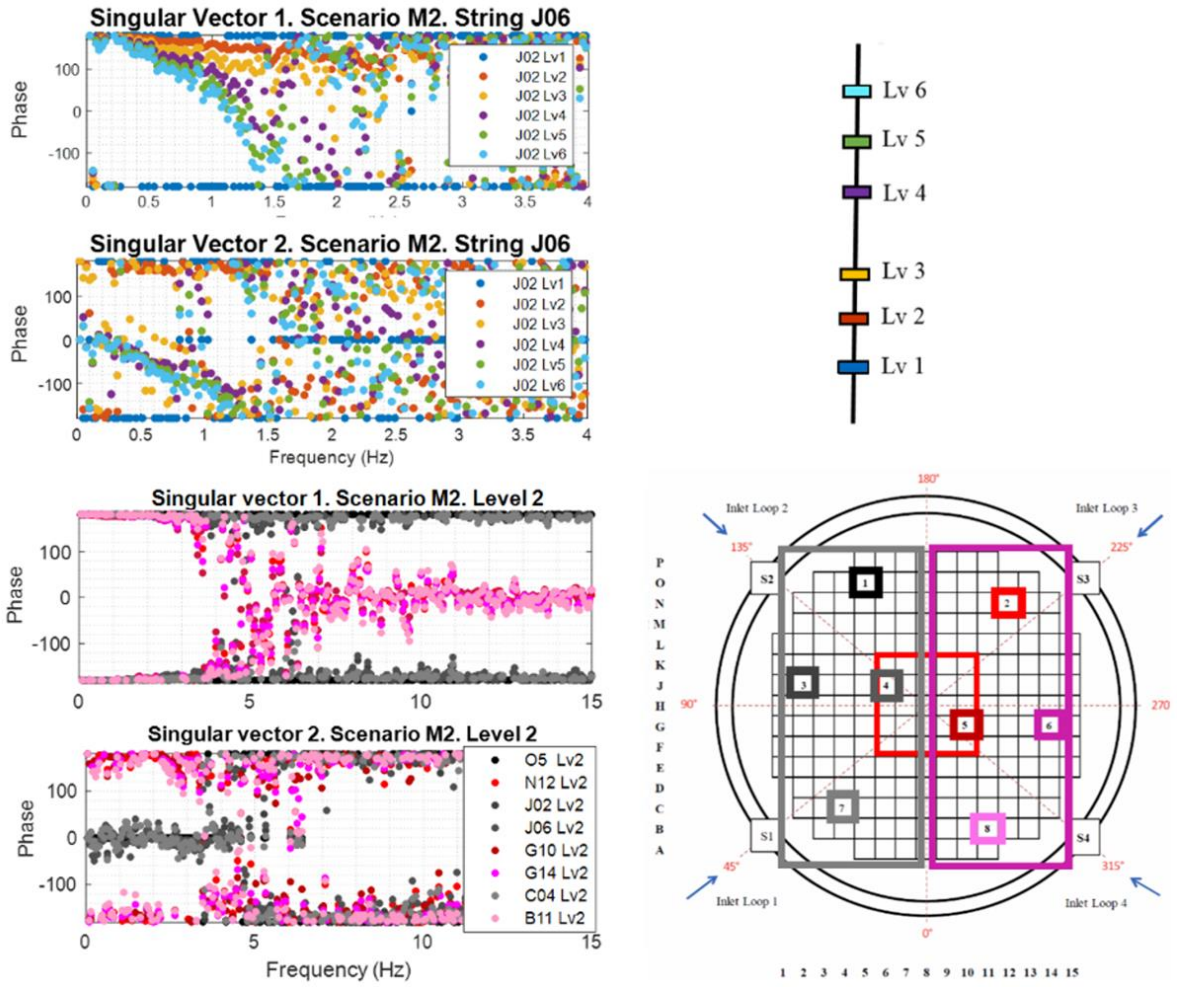

Figure 12: Singular vectors 1 and 2 of the scenario with temperature and flow fluctuations with random vibrations. Radial analysis upper side and axial analysis in the lower side.

6.3. Sensitivity analysis to variation of the perturbation amplitude

The following analysis illustrates the changes observed when the amplitude of one type of perturbation is modified whilst the rest of perturbations keep constant. In other words, a sort of sensitivity analysis is performed to relate the change between the amplitude of the perturbations to the changes observed in the singular values and the singular vector phases

6.3.1. Sensitivity to FA random vibration amplitude

This subsection compares two scenarios with the same thermal-hydraulic perturbation (±1 ºC, ±1 %), but with two different amplitudes in the random vibrations, in the first case 0.5 mm and in the second case 1 mm.

Figure 13 shows the axial and radial analysis of Singular values 1 and 2. In each graphic, we have two scenarios with the same temperature and flow fluctuation, but with two types of random vibrations (0.5 mm and 1 mm), axial analysis in the left-hand side, radial analysis in the right-hand side. We can appreciate in both analyses that the horizontal part of the singular value 1, above 5 Hz, increases with the increase of amplitude vibration. In

the low frequency range, the radial analysis exhibits the effect of the FA random vibrations amplitude variation on the second singular value.

In both comparisons, the non-horizontal sections below 3 Hz are overlapped. These sections follow the typical response due to thermal-hydraulic fluctuations, which has been kept constant, which confirms again the full dominance of the such fluctuations in comparison to FA vibrations.

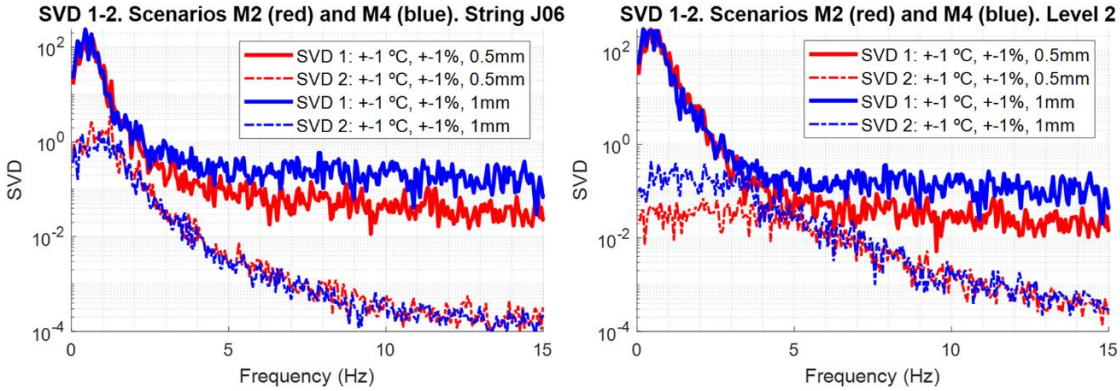

Figure 13: Comparison of singular values 1 and 2 of the scenarios with thermal-hydraulic fluctuation and random vibrations (0.5mm and 1mm). Axial analysis in the left-hand side. radial analysis in the right-hand side

Regarding the singular vector, Figure 14 shows the axial analysis of the singular vectors 1 and 2 in the scenarios with combination of thermal-hydraulic fluctuations (±1 ºC, ±1 %) and random vibrations (0.5 mm left-hand side and 1mm right-hand side). Comparing both scenarios, the following can be mentioned:

- All the phases in the singular vector 1 present a clearly linear slope in the low-frequency range.
- Note that the resultant slope resembles to that of the temperature fluctuation scenario. The increase of the random vibration amplitude reduces the slope very slightly in both singular vectors 1 and 2.
- The increase in the amplitude vibrations makes the phases of the second singular vector noisier.
- In the case of the radial analysis, there are no differences between the two cases, all the cases follow the same distribution as seen in section 6.2.1, Figure 12 lower side.

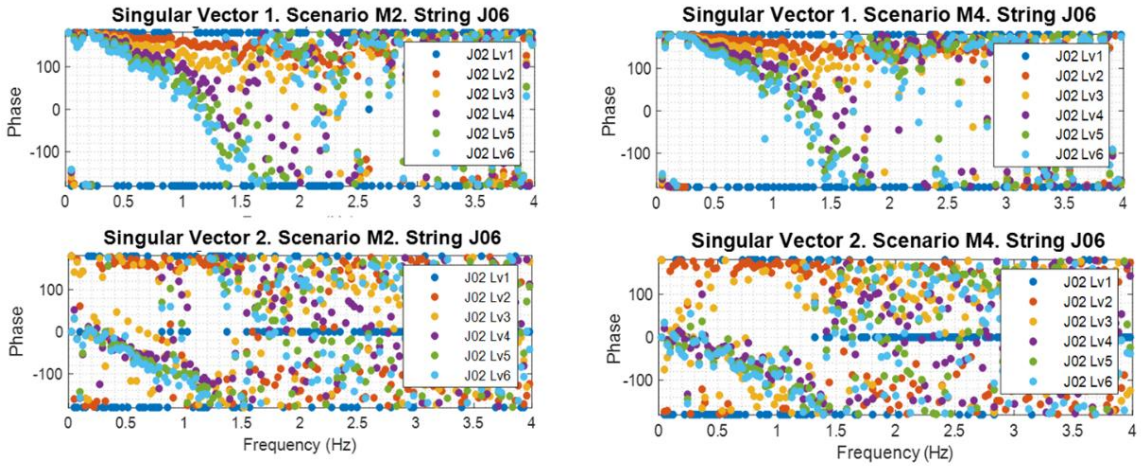

Figure 14: Axial analyses of the singular vectors 1 and 2 in the scenarios with thermal-hydraulic fluctuation and random vibrations. 0.5mm in the left-hand side and 1mm in the right-hand side).

6.3.2. Sensitivity to thermal-hydraulic fluctuation amplitude

This subsection compares three scenarios with the same amplitude in the FA random vibrations, 1 mm, but different amplitudes in the thermal-hydraulic perturbations, M3 (±3 ºC, ±1 %), M4(±1 ºC, ±3 %), and M5 (±1 ºC, ±1 %).

Figure 15 shows the singular values 1 and 2 in the three mentioned scenarios. The axial analysis is in the left-hand side, and the radial analysis in the right-hand side.

In frequency range below 2 Hz, the singular value 1 is higher in the scenario with higher temperature oscillations (±3 ºC). We can also appreciate that the difference between the singular value 1 of the scenarios M3 (red line) and M4 (black line) is very little in contrast to that between M4 and M5 (red line). This indicates that the increase of temperature oscillations produces larger amplitude differences.

In both plots of both scenarios, the horizontal sections (above 3 Hz) are overlapped, as expected, since the mechanical vibration amplitude was kept constant.

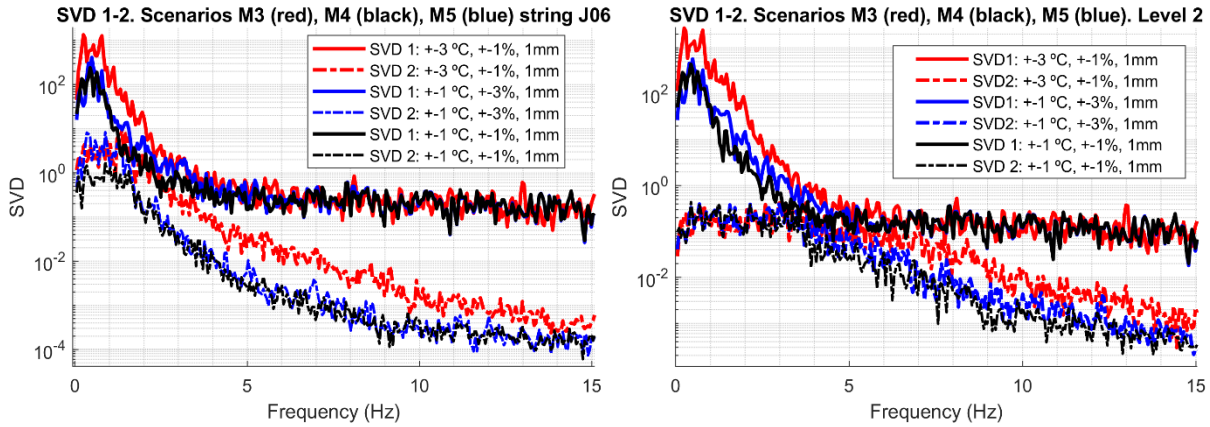

Figure 15: Comparison of singular values 1 and 2 of the scenarios with random vibrations and thermal-hydraulic fluctuation: M3 (±3 ºC, ±1 %), M4 (±1 ºC, ±1 %), and M5 (±1 ºC, ±3 %). Axial analyses in the left-hand side. radial analyses in the right-hand side.

Regarding the singular vector analysis, Figure 16 shows the axial analysis of the singular vectors 1 and 2 in three scenarios with random vibrations, 1 mm for all cases and thermal-hydraulic fluctuation: ±3 ºC, ±1 % left-hand side, ±1 ºC, ±1 % middle, and ±1 ºC, ±3 % right-hand side. Comparing the three scenarios, we can mention:

- All the phases in the singular vector 1 present a linear slope in the low-frequency range.
- The increase of temperature oscillation amplitudes increases the slope in both singular vectors 1 and 2.
- In the case of the radial analysis, not shown here, there were no differences between the three cases, all the cases follow the same distribution seen in section 6.2.2, Figure 12 lower side.
- As can be seen in Figure 16, right subplot, when the amplitude of the flow fluctuations reaches a certain value, their effects are predominant, that is, we have a low slope in the linear phase.
- The second singular vector does not show patterns that add recognisable information.

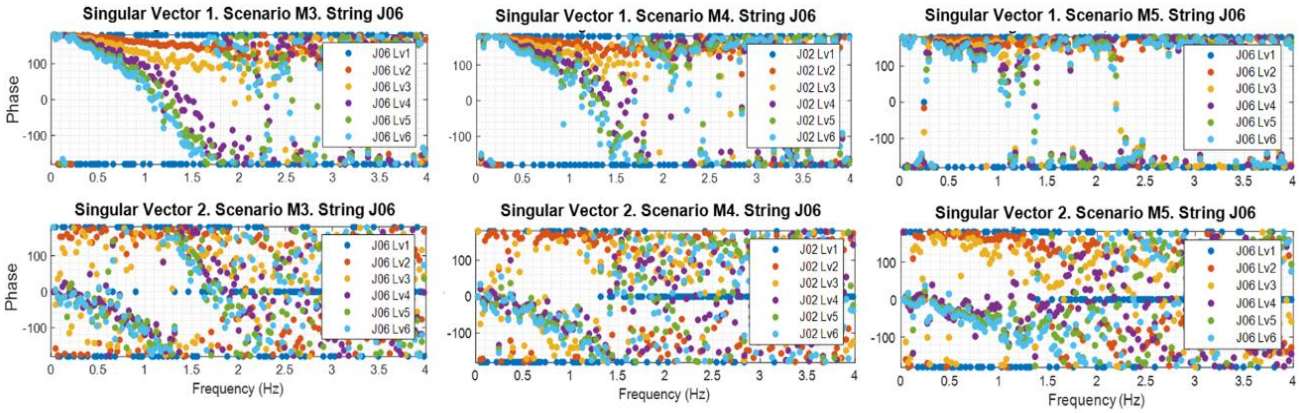

Figure 16: Axial analyses of the singular vectors 1 and 2 in the scenarios with thermal-hydraulic fluctuation and random vibrations. 0.5mm in the left-hand side and 1mm in the right-hand side).

6.4. Scenarios with FA coloured vibrations

In this subsection, the results from two scenarios with FA colored vibrations are presented. The first scenario presented only considers individual 1.5 Hz FA vibrations. In Figure 17 there are three subfigures; on the left-hand side, the singular values are shown, on the right-hand side, the singular vector one and two phases are plotted. The following comments can be added:

- The singular value 1 shows a non-damped resonance at 1.5 Hz with a very high amplitude which represents the input FA vibration. There are other resonances with lower amplitudes located at frequency multiples of 1.5 Hz (3, 4.5, 6…Hz).
- The singular vector 1 plot shows out of phase for that frequency.

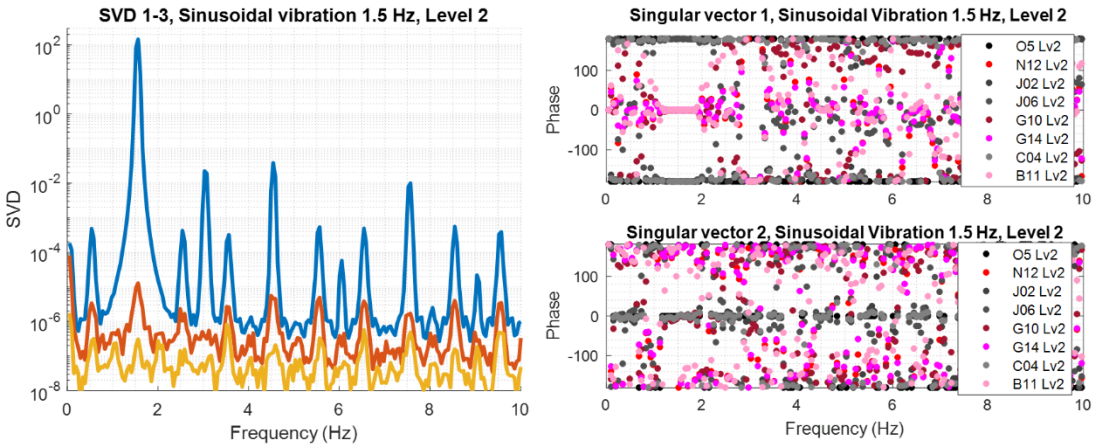

Figure 17: Singular values 1-3 (left-hand side) and phase distribution of singular vectors 1and 2 (right-hand side) for a scenario with sinusoidal vibrations of 1.5 Hz of the central cluster.

In Figure 18, the results of a mixed scenario with 1.5 Hz FA colored vibrations are presented. The thermal-hydraulic perturbations consists of ±1 ºC and ±1 % flow. The following comments can be drawn:

- In the left subfigure, the singular values show:
  - Below 1 Hz, singular value 1 is predominant.
  - In the vicinity of 1.5 Hz, both singular values 1 and 2 present a resonance at 1.5 Hz.

In singular vector 1 there is out of phase at 1,5 Hz. In singular vector 2 all detectors are in phase for 1.5 Hz. This means the effect of the fuel assemblies vibration lies on singular value 1 and singular vector 1.

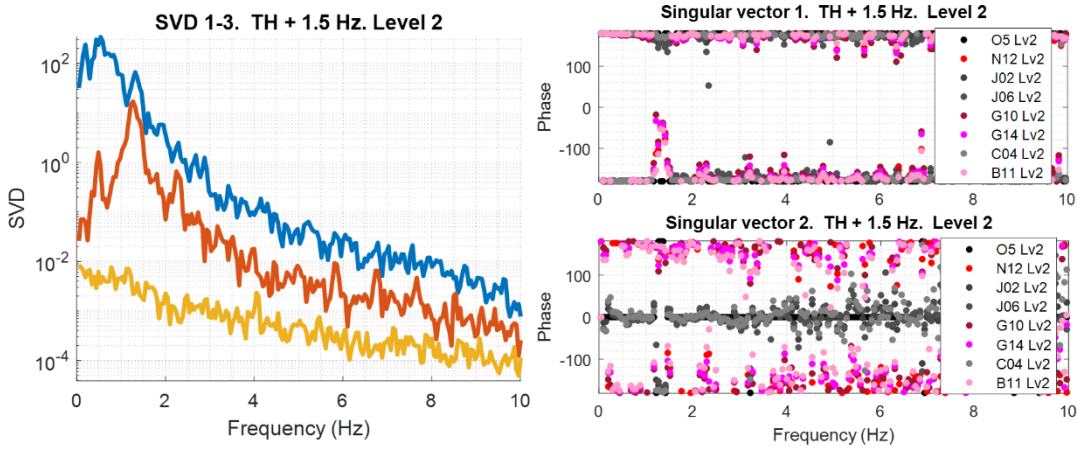

Figure 18: Singular values 1-3 (left-hand side) and phase distribution of singular vectors 1and 2 (right-hand side) for a scenario with sinusoidal vibrations of 1.5 Hz of the central cluster and thermal-hydraulic fluctuations (±1 ºC and ±1 %) temperature and flow respectively

7. DISCUSSION

In the previous section the results were presented divided into four subsections that consider scenarios with a crescent complexity in terms of perturbations. This section discusses the observations carried out in the results section and the performance and

feasibility of the OMA (FDD) to infer perturbation characteristics from the neutron noise response.

7.1. Amplitude, linear phase and out-of-phase relationship

In (Torres et al. 2019) the possible phenomena associated with three main neutron noise spectral characteristics were pointed out. These were: the high amplitude below 1 Hz mainly due to temperature fluctuations, the low slope in the linear phase due to flow fluctuations, and the out-of-phase relationship in opposite detectors because of the random vibrations of a cluster of fuel assemblies in the center of the core.

As seen in section 6.1, the proposed methodology allows us to make a series of observations that point out in the same direction.

Singular values provide information about the response amplitude in the frequency domain due to each perturbation. In Figure 5 and Figure 7 we have seen the different shapes of the singular values obtained when one type of perturbations is assumed: temperature and flow fluctuation in Figure 5, and FA random vibrations in Figure 7. Essentially, the response of the scenarios in Figure 5 differ in magnitude, however, both have a very similar shape in contrast to the case of FA random vibrations, whose singular values (Figure 7) shows an almost constant value in all the frequency range.

Singular vectors give us information about the phase spatial distribution of every detector involved in the analysis. In Figure 6, we could see that scenarios with temperature or flow fluctuations present, in axial analysis, different linear slopes in the low-frequency range, but equal behaviour in the radial analysis. We can say that they are similar to each other compared to the scenarios with random vibrations shown in Figure 8. In the case of the FA random vibrations of a central cluster, the axial distribution shows that all the detectors are in phase. This happens in all the strings, which means that the transport phenomenon associated is attributed only to the thermal-hydraulic fluctuations. In the case of the radial analyses at all levels, it is remarkable that the reactor is divided into two halves in out-of-phase.

As a consequence, the features observed in the singular values and singular vectors allow us to differentiate and characterize the perturbations that take place in each individual scenario, this is a fundamental step in the process of understanding the phenomenon, however, real data is a composition of multiple types of perturbations, what increases the problem complexity.

At last, regarding the effect of coloured FA vibrations on the response, it is possible to see that the singular value 1 present a resonance at the frequency of the vibration. The singular vector 1 also shows the usual out of phase behaviour when a cluster of fuel elements vibrate. Even, when there are thermal-hydraulic perturbations, the mechanical vibration presents itself in the first singular value and therefore, it is a predominant phenomenon in the neutron response.

7.2. Decomposing the neutron noise response

In real plant data, the use of OMA techniques requires a series of assumptions about the statistical character of the input excitation, since they are not exactly known. Usually, Gaussian distribution and white noise are assumed. In the simulations we do not have this concern, we know all the perturbations characteristics that are assumed in all the scenarios. So, this fact allows us to assess the feasibility of OMA to infer characteristics of the input excitation from the neutron noise data in PWR.

In Figure 19, the left-hand subplot shows the APSD (response) of the three basic types of perturbations (±1 ºC, ±1 % and 1 mm). On the right-hand subplot, we can see the resultant response due to the action of the three individual perturbations at the same time (scenario M4).

Figure 20 on the right shows the results obtained when OMA methodology is applied to M4 scenario the singular values in the upper side and the singular vectors in the lower side. The result obtained is a decomposition of the traditional APSD shown in the left-hand side of the figure.

In Figure 19 left-hand side, note that the nature of the response due to each individual perturbation is very different. On the one hand, temperature and flow fluctuation behave similarly mainly in the low-frequency range. On the other hand, FA random vibrations present an almost constant response. The common nature of the two thermal-hydraulic cases explains and justifies the FDD results. We can notice that the temperature and flow fluctuation response are included in the same singular value, see Figure 20, upper side.

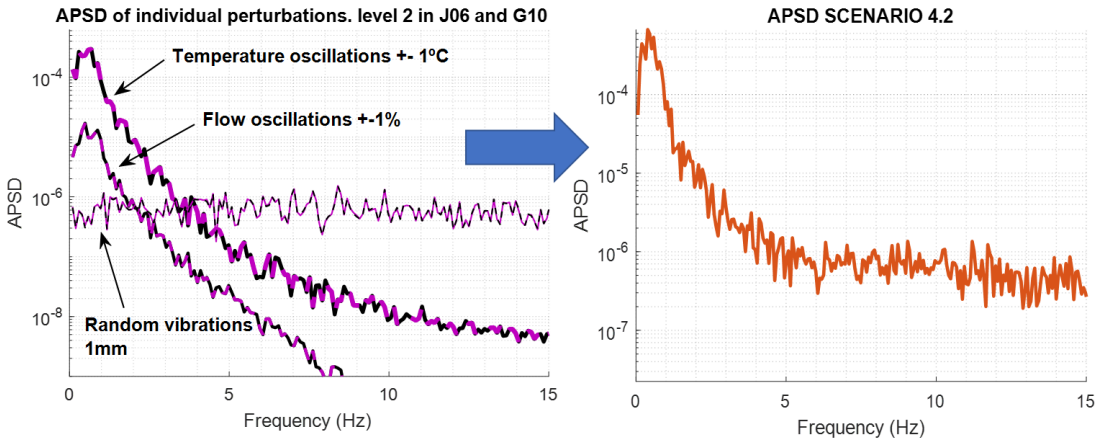

Figure 19: The APSD of the three basic types of perturbations; Temperature and flow fluctuation, and FA random vibrations (left-hand side). The APSD of a scenario where the three types of perturbation were assumed (right-hand side).

In Figure 20, we can appreciate that both singular values and singular vectors exhibit two zones clearly defined. The first zone extends up to approximately 4 Hz, while the second zone starts just above 6 Hz. In between, we have a transition zone.

The singular value 1 and singular vector 1 follow the same distribution. Observing the singular value 1:

- In the first zone we have the peak.
- In the second zone we have the horizontal section.

Observing the singular vector 1:

- In the first zone all the detectors have the same phase.
- In the second zone, the phases are separated into two groups that divide the reactor into two halves in out-of-phase.

We can conclude that the first zone corresponds to the thermal-hydraulic fluctuations, and the second zone corresponds to the random vibrations. This partial separation or phenomena distribution also occurs with the singular value 2 and singular vector 2, but in a opposite way. In this case, the first zone is related to the FA random vibration, while the second zone is associated to the thermal-hydraulic fluctuations. To illustrate better this separation in components, in Figure 20, right side, we can see highlighted in yellow the thermal-hydraulic component and in green the mechanical vibration component for each singular value (upper side) and singular vector (lower side).

As mentioned in section 6.2, the axial analysis presents a very similar phenomenon distribution to the radial one, but it is important to note that the two zones (first zone below 3 Hz and above 6 Hz) are related to the detectors selected in the analysis. For example, in the axial analysis, the response amplitude due to the vibrations is larger than that in the radial analysis. This is because all the detectors of the string J06 are inside the vibrating cluster.

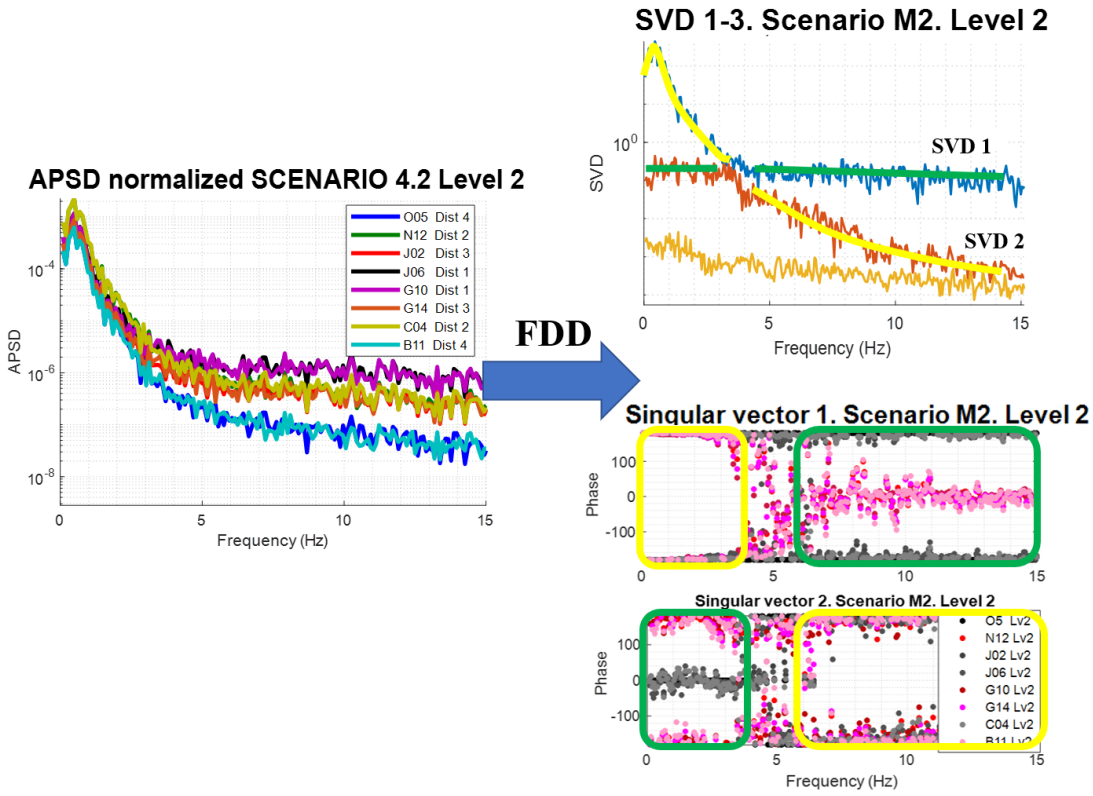

Figure 20: Radial analysis with the eight detectors of the level 2, singular values 1 to 3 in the upper side and the first two singular vectors in the lower side. In the right side, highlighted in yellow the thermal-hydraulic component and in green the mechanical vibration component

7.3. Inferring perturbation characteristics from the response

The decomposition of one scenario in singular values and singular vectors presented in section 6.2 is one of the possibilities to characterise the involved phenomena. Another possibility was presented in Section 6.3. where scenarios with multiple perturbations but differing in the amplitude of only one type of perturbations are compared. This allows us to observe the relative influence of modifying one type of perturbation at a time.

We have to note the difficulty of analysing the response from different types of phenomena at the same time. Although temperature and flow oscillations are very similar in response, they cannot be directly compared in a quantitative way. Therefore, comparing scenarios where only one type of perturbation amplitude is modified allows performing a sensitivity analysis. This approach exhibits suitable capabilities to observe the resultant relationship between the changes in the input perturbation amplitude and the final neutron noise response.

Figure 21 presents the singular values 1 and 2 in radial analyses. On the left-hand subplot when only FA random vibration amplitude is modified, while the right-hand subplot corresponds to when only thermal-hydraulic oscillations are modified.

We can easily distinguish the direct relation when one type of perturbation is increased. The singular value sections that exhibit increase are highlighted in yellow. Note that the higher the amplitude of the vibration, the higher the value of the singular value 1 above 6 Hz, see in Figure 21 left-hand subplot. And, the higher the temperature oscillations amplitude, the higher the singular value 1 below 2 Hz, see Figure 21 right-hand subplot. In the case of Fourier analysis, regarding the APSD, the effect of the mechanical vibrations is appreciable mainly when the sensor is located near the source of perturbations, but it is not if the detector is far away. In the case of the current methodology, it gathers all the information from all the detectors as a whole.

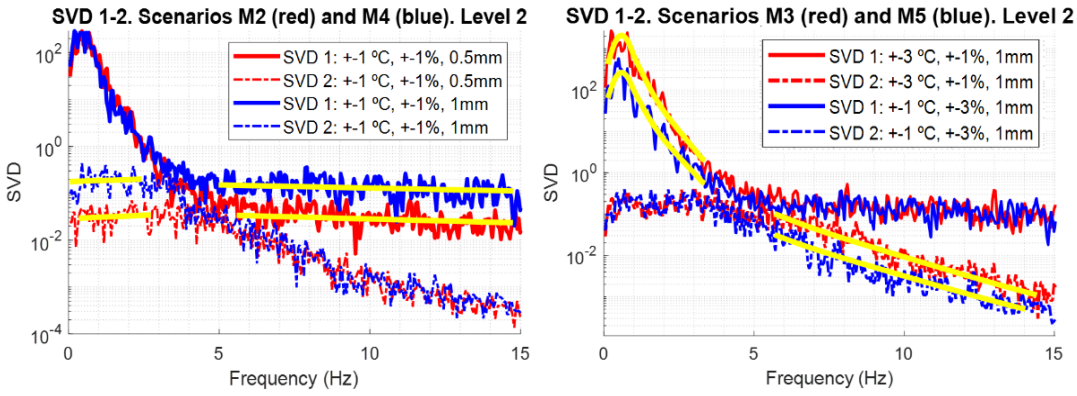

Figure 21: Comparison of singular values 1 and 2 axial analyses. In the left-hand side, scenarios with thermal-hydraulic fluctuation and random vibrations (0.5mm and 1mm). In the right-hand side random vibrations and thermal-hydraulic fluctuation (±3 ºC, ±1 %, and ±1 ºC, ±3 %).

Regarding the singular vectors, in the axial analysis shown in Figure 16, we can notice the clear evolution of the linear slope as the thermal-hydraulic perturbation ratio changes the slope of the linear phase . That is, the higher the flow perturbation amplitude, the

lower the slope of the linear phase observed in the singular vectors. The second singular vector shows a similar trend, but the graph is quite noisy.

7.4. Further considerations of the methodology

As mentioned in section 5, In the use of the Modal analysis approach, we must take into account some particularities of the phenomenon e.g., we do not study vibrations as a response, but the response of neutron noise. And, we have no structural mode shapes (mechanical vibrational modes), but neutron noise phase distribution. So, it is fundamental to have in mind that the method has been imported from the structural dynamical analysis field in order to be able to interpret correctly the results.

In all the simulations, as in real data, we obtain a large number of signals in the time domain. Each set of signals is a spatial map of the response to the input perturbations. Findings suitable ways to tackle all the information is critical so that we can study the phenomenon in an efficient way. Keeping in mind these particularities of the data, we can remark three important advantages and strengths of the methodology:

- The effectiveness in the multi-variable and spatial analysis
- It allows distinguishing different responses of the system to different physical causes in the same frequency region
- The capability to condense a large amount of information plotting a couple of singular values or singular vectors

In the case of these simulations, the responses spectra do not have dominating peaks, except the heavily damped resonance peak below 1 Hz that obeys to thermal-hydraulic excitation inputs. We do not have any other resonance.

In real cases, we can find resonances in the high-frequency range, these resonances are caused by mechanical mechanisms like the rotation of the pumps and vibrational modes of the core vessel (Dykin et al. 2013, 2014; Montalvo et al. 2016; Pázsit et al. 2019).

8. CONCLUSIONS

In this paper the OMA methodology, concretely the FDD, was performed on a series of neutron noise signals from simulated scenarios based on the transient nodal code S3K. The scenarios were analysed from the point of view of characterizing the thermal-hydraulic and mechanical perturbations. To this aim, the simulations were analysed in three steps according to the complexity of the simulated perturbations: First, scenarios with only one type of perturbation, second, scenarios with multiple types of perturbations, and finally, scenarios with different ratios in the perturbation amplitudes.

The results illustrate the effectiveness of the methodology to separate the response due to mechanical vibrations and thermal-hydraulic fluctuation in all the frequency range. The method decomposes the signal in the frequency domain into singular values and singular vectors. On one hand, the singular values establish a hierarchy of the dominant phenomenon taking place at a particular frequency range. The bigger the singular value, the more dominant is the phenomenon. On the other hand, the modulus and phases

observed in the singular vectors have strong analogies with the traditional calculation of the coherence and phase relationships. The difference is that OMA allows distinguishing different phenomena taking place at an equal frequency range. The separation of phenomena cannot be performed with Fourier analysis or HHT.

Regarding the analysis, we can highlight a series of features that allow us to infer the nature of the perturbations that take place in the scenarios.

- Temperature fluctuation characterization: the higher the fluctuation, the higher the first singular value below 2 Hz.
- Mechanical vibration characterization: the higher the vibration amplitude, the higher the horizontal sections, in singular value 1 above 6 Hz, and singular value 2 below 3 Hz.
- When the mechanical vibration is coloured, it presents itself as a resonance in the singular value one and with an out of phase behaviour in the singular vector 1.
- Flow perturbation characterization: the higher the flow perturbation amplitude, the lower the slope (due to the instantaneous propagation of the perturbation) in the linear phase of the first singular vectors below 2 Hz when axial analysis is performed.

It is also important to mention the following:

- The partial separation of the two phenomena (thermal hydraulic and mechanical vibrations) in the first two singular values occurs in an opposite way.
- The phase separation in all the frequency range with the singular vectors 1 and 2 in a supplementary way allows define the phase distribution of all the detectors in all the frequency range.
- There was an effective identification of transport phenomena associated to the thermal-hydraulic phenomena.

The present study shows that OMA is a powerful tool to infer characteristics of the input excitation from the neutron noise signals in PWR. It extracts information from the data that other techniques such as Fourier based methods or HTT are not able to do. Usually, the FDD methodology is used to identify different resonances. However, in the current simulated data, there are not many resonances clearly defined. The only resonance that we have is the thermal-hydraulic feedback below 1 Hz and the 1.5 Hz FA vibration. In future work, it would be desirable to use the Modal Assurance Criterion (MAC) (Pastor et al. 2012) to indicate the similarity between singular vectors and to link this with a particular physical phenomenon. Besides, the methodology should be tested in real plant data.

ACKNOWLEDGEMENTS

The research leading to these results has received funding from the Euratom research and training programme 2014-2018 under grant agreement No 754316 (Project CORTEX Core Monitoring Techniques Experimental Validation and Demonstration).

REFERENCES

Batel, M. and B. Norcross. 2002. “Operational Modal Analysis - Another Way of Doing Modal Testing.” *S V Sound and Vibration* 22–27.

Bermejo, J. A. 2015. “Noise Analysis in PWR. PHD Thesis.” Universidad Politécnica de Madrid.

Bermejo, J. A., C. Montalvo, and A. Ortego. 2017. “On the Possible Effects Contributing to Neutron Noise Variations in KWU-PWR Reactor: Modelling with S3K.” *Progress in Nuclear Energy* 95.

Brincker, R., L. M. Zhang, and P. Andersen. 2000. “Modal Identification from Ambient Responses Using Frequency Domain Decomposition.” Pp. 625–30 in *IMAC-XVIII: A CONFERENCE ON STRUCTURAL DYNAMICS*. Vol. 4062.

Chionis, D., A. Dokhane, L. Belblidia, H. Ferroukhi, G. Girardin, and A. Pautz. 2020. “Development and Verification of a Methodology for Neutron Noise Response to Fuel Assembly Vibrations.” *Annals of Nuclear Energy*.

Chionis, D., A. Dokhane, L. Belblidia, M. Pecchia, G. Girardin, H. Ferroukhi, and A. Pautz. 2017. “SIMULATE-3K Analyses of Neutron Noise Response to Fuel Assembly Vibrations and Thermal-Hydraulics Parameters Fluctuations.” in *International Conference on Mathematics & Computational Methods Applied to Nuclear Science & Engineering*. Jeju.

Chionis, D., A. Dokhane, H. Ferroukhi, G. Girardin, and A. Pautz. 2018a. “PWR Neutro Noise Phenomenology: Part II - Qualitative Comparison against Plant Data.” Pp. 1001–12 in *PHYSOR 2018: Reactor Physics Paving The Way Towards More Efficient Systems*.

Chionis, D., A. Dokhane, H. Ferroukhi, G. Girardin, and A. Pautz. 2018b. “PWR Neutron Noise Phenomenology: Part I - Simulation of Stochastic Phenomena with SIMULATE- 3K.” Pp. 1001–12 in *PHYSOR 2018: Reactor Physics Paving The Way Towards More Efficient Systems*.

Czibók, T., G. Kiss, S. Kiss, K. Krinizs, and J. Végh. 2003. “Regular Neutron Noise Diagnostics Measurements at the Hungarian Paks NPP.” *Progress in Nuclear Energy* 43(1):67–74.

Demazière, C. 2011. “CORE SIM: A Multi-Purpose Neutronic Tool for Research and Education.” *Annals of Nuclear Energy*.

Dykin, V., C. Montalvo, H. Nylén, and I. Pázsit. 2013. *Ringhals Diagnostics and Monitoring, Annual Research Report 2013*.

Dykin, V., C. Montalvo, H. Nylén, and I. Pázsit. 2014. *Ringhals Diagnostics and Monitoring , Final Research Report 2012-2014*.

Fry, D. N., J. March-Leuba, and F. J. Sweeney. 1984. *Use of Neutron Noise for Diagnosis of In-Vessel Anomalies in Light-Water Reactors*.

Greiner, G. 2008. “Operational Modal Analysis and Its Application for SOFIA Telescope Assembly Vibration Measurements.”

Hashemian, H. M. 2006. *Maintenance of Process Instrumentation in Nuclear Power Plants Power Systems*. Springer.

Hashemian, H. M. 2011. “On-Line Monitoring Applications in Nuclear Power Plants.”

Progress in Nuclear Energy 53(2):167–81.

Kozlowski, T. and T. J. Downar. 2003. *OECD/NEA and US NRC PWR MOX/UO2 Transient Benchmark Nº 2*.

Montalvo, C., I. Pázsit, H. Nylén, and V. Dykin. 2016. "First Evidence of the Pivotal Motion ('tilting Mode') of the Core Barrel in the RINGHALS-4 PWR." *Physics of Reactors 2016, PHYSOR 2016: Unifying Theory and Experiments in the 21st Century* 4:2571–79.

Olmo-Juan, N., C. Demazière, T. Barrachina, R. Miro, and G. Verdu. 2019. "PARCS vs CORE SIM Neutron Noise Simulations." *Progress in Nuclear Energy*.

Pastor, M., M. Binda, and T. Harčarik. 2012. "Modal Assurance Criterion." Pp. 543–48 in *Procedia Engineering*. Vol. 48.

Pázsit, I., L. A. Torres, C. Montalvo, Y. Kitamura, L. Nagy, and H. Nylén. 2019. *Ringhals Diagnostics and Monitoring, Annual Research Report 2018-2019*.

Rainieri, C. and G. Fabbrocino. 2015. *Operational Modal Analysis of Civil Engineering Structures*.

RSK/ESK. 2013. "PWR Neutron Flux Oscillations. Statement." in *457th RSK meeting*.

Runkel, J. 1987. "Noise Analysis in Pressurized Water Reactor."

Seidl, M., K. Kosowski, U. Schüler, and L. Belblidia. 2015. "Review of the Historic Neutron Noise Behavior in German KWU Built PWRs." *Progress in Nuclear Energy* 85:668–75.

Spanish Nuclear Safety Council, 2011. 2011. *Technical Judgement Proposal. Application of 50 Revision of the Technical Especification of Operation of Trillo NPP (in Spanish)*.

Torres, L. A., D. Chionis, C. Montalvo, A. Dokhane, and A. García-Berrocal. 2019. "Neutron Noise Analysis of Simulated Mechanical and Thermal-Hydraulic Perturbations in a PWR Core." *Annals of Nuclear Energy* 126:242–52.

Torres, L. A., D. Chionis, C. Montalvo, A. Dokhane, and A. García-Berrocal. 2020. "Neutron Noise Spectral Features of Simulated Mechanical and Thermal-Hydraulic Perturbations in a PWR Core." in *PHYSOR 2020*.

Tran, H. N., I. Pázsit, and H. Nylén. 2015. "Investigation of the Ex-Core Noise Induced by Fuel Assembly Vibrations in the Ringhals-3 PWR." *Annals of Nuclear Energy* 80:434–46.

Viebach, M., N. Bernt, C. Lange, D. Hennig, and A. Hurtado. 2018. "On the Influence of Dynamical Fuel Assembly Deflections on the Neutron Noise Level." *Progress in Nuclear Energy* 104:32–46.

Viebach, M., C. Lange, N. Bernt, M. Seidl, D. Hennig, and A. Hurtado. 2019. "Simulation of Low-Frequency PWR Neutron Flux Fluctuations." *Progress in Nuclear Energy*.